Self-Diffusion Studies of Binary Mixtures in NaX Zeolites Using Pulsed Field Gradient NMR and a Maxwell−Stefan Model†

Qi Zhao and Randall Q. Snurr*

Department of Chemical and Biological Engineering and Institute for Catalysis in Energy Processes, Northwestern University, 2145 Sheridan Road, Evanston, Illinois 60208

Received: November 15, 2008; Revised Manuscript Received: January 21, 2009

Intracrystalline self-diffusion coefficients were measured by pulsed field gradient (PFG) NMR for single components and binary mixtures of CF_4 and various hydrocarbons in large-crystal NaX zeolites. A short-time diffusion model was used to obtain the unrestricted intracrystalline self-diffusivities by extrapolating to zero diffusion time, when no molecules can leave the crystal during the measurement. The results were used to test a theoretical model from Skoulidas, Sholl, and Krishna for predicting diffusion coefficients of mixtures in zeolites from single-component data. The predicted binary self-diffusivities are consistent with those directly measured in PFG NMR mixture experiments, thus providing an experimental validation of the model.

1. Introduction

Intracrystalline diffusion can play an important, even rate-limiting, role in zeolite applications such as catalysis, membranes, and adsorption separations.[1,2] The regular networks of pores also make zeolites interesting model systems for understanding molecular motion and diffusion in confined environments. There have, therefore, been many studies of diffusion in zeolites, using experiments, atomistic simulation, lattice models, and theory. Practical applications always involve at least two different components, but understanding of multicomponent diffusion in zeolites is still limited, and experimental data are scarce. Chen and Yang[3] provide a summary of experimental studies of multicomponent diffusion in zeolites up to about 1996. Recently, there have been several studies using pulsed field gradient (PFG) NMR to measure self-diffusivities in binary mixtures. The systems examined include ethane/ethylene in NaX[4] and in silicalite,[5] methane/ethylene in NaY,[5] methane/benzene in NaY,[6] methane/CF_4 in silicalite,[7] and methane/xenon in silicalite.[8] Schuring et al.[9] used a tracer-exchange positron emission profiling technique to measure self-diffusivities for *n*-hexane/2-methylpentane mixtures in silicalite, and Gergidis et al.[10] reported results for methane/*n*-butane in silicalite from quasielastic neutron scattering. A general conclusion from these studies is that faster species are slowed in the mixtures and that the difference in self-diffusivities between the components is smaller in the mixtures than for the pure components. The magnitude of these effects depends on the zeolite pore topology, the presence of cations, and the loading and nature of the adsorbed molecules.

Efforts have also been made to measure transport in binary systems under nonequilibrium conditions.[3] Recently, binary mixtures of ethane, *n*-butane, and isobutane in MFI zeolites were studied under co- and counter-diffusion conditions using the zero length column (ZLC) method.[11] Brandani et al.[12] used ZLC to examine mixtures of benzene and two xylene isomers in silicalite and compared the response curves to those predicted by two simple models. In general, it is difficult to measure the elements of the binary Fickian diffusion tensor, although a few reports exist in the literature.[13,14]

The elements of the multicomponent Fickian diffusion tensor for a given system may depend on the total loading of adsorbed molecules, the adsorbed-phase composition, and the temperature. Given the difficulties in measuring multicomponent diffusion coefficients, it would be useful to have predictive models to calculate the multicomponent diffusion coefficients from single-component data. Several models have been proposed for this purpose.[3,15−18] However, given the lack of experimental data, it has been hard to test how widely applicable they are. In this Article, we report a systematic set of self-diffusivity data for binary mixtures of CF_4 adsorbed in NaX zeolite with *n*-alkanes of various lengths, cyclohexane, and benzene. We use these data to test the recent model of Skoulidas, Sholl, and Krishna.[17] While the Fickian diffusion coefficients are most useful for design of equipment and processes, the self-diffusion coefficients provide more information on correlation effects[19] and are not affected by the sorption thermodynamics. In addition, the self-diffusivities can be used to test molecular simulations more easily, because the self-diffusivities are easier to calculate from simulations.[20,21]

PFG NMR measures self-diffusion on a time scale of milliseconds or longer and a length scale of micrometers to millimeters. Although large-crystal zeolites can be synthesized with particle diameters around tens of micrometers, in general some molecules will diffuse to the edge of a crystal during the time of a PFG NMR measurement, even for large zeolite crystals.[22−25] Care must, therefore, be taken in determining a self-diffusion coefficient that is independent of the edge effects. Only when the diffusion time is near zero can the effects of the external surfaces be neglected.[22−25] Some recent papers have presented strategies to obtain the self-diffusivity at zero diffusion time (indicated as D_0 in this Article),[22,25−28] and we used the short-time diffusion model of Mitra et al.[23,24] Diffusivities of the individual components of the mixtures were obtained by using the ^{19}F frequency for CF_4 and the ^1H frequency for the other species.

† Part of the "George C. Schatz Festschrift".

* Corresponding author. Tel.: (847) 467-2977. Fax: (847) 467-1018. E-mail: snurr@northwestern.edu.

10.1021/jp810058z CCC: $40.75
Published on Web 03/02/2009

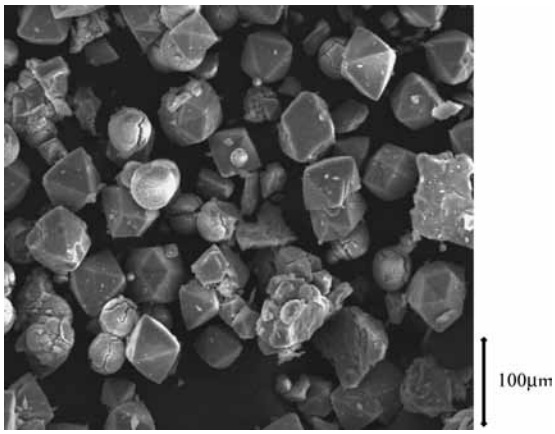

Figure 1. SEM image of calcined NaX zeolites.

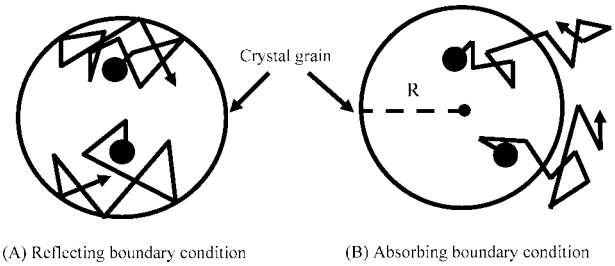

Figure 2. Schematic diagrams of two limiting boundary conditions for molecular diffusion in nanoporous particles with average radius R. The "●" denote the adsorbed molecules at $t = 0$, and the solid lines denote their diffusion paths.

2. Experimental Methods

The large-crystal NaX zeolite sample was synthesized using triethylamine and was kindly provided by George T. Kokotailo. The ratios of Si/Al and Na/Al in the sample are 1.27 and 0.86, respectively, as measured in our laboratory. For large crystals, uneven heating during calcination can lead to defects and cracks in the crystals. Therefore, the following procedure was used for the calcination. First, the as-synthesized sample was slowly heated to 393 K at a rate of 0.5 K/min and held for 2 h at this temperature. Next, the temperature was further elevated to 823 K at the same rate. After 7 h at 823 K, the sample was cooled back to room temperature at the same rate. Figure 1 shows the SEM image of the calcined sample. The regular octahedral crystals indicate that the slow calcination procedure did not damage the crystals. The radii of the crystals are as large as 35 μm. The spherical particles visible in the image are zeolite P, as indicated by X-ray diffraction analysis of the samples. Zeolite P is a dense material with pores that are too small for molecules to enter. This impurity should, therefore, not affect the results of this study.

NMR samples were prepared by packing a known amount of the calcined sample into a glass NMR tube with a 5 mm outer diameter (Wilmad 503-PS-8). The height of the sample in the NMR tube was similar to that of the gradient coil located in the NMR probe. Samples were dehydrated by attaching them to a vacuum line and heating at a rate of 0.25 K/min to 393 K and holding for 4 h to remove most of the adsorbed water. Next, the samples were heated to 723 K at a rate of 0.4 K/min, and the vacuum reached 10^{-6} torr. This condition was maintained for 12 h, and then the sample was slowly cooled back to room temperature at a rate of 0.5 K/min.

The sorbates included CF_4 and various hydrocarbons as second components. They were quantitatively introduced into the dehydrated samples in sequence from the gas phase by submerging the sample tube in a liquid nitrogen bath. The sample tubes were then immediately sealed using a torch. The exact amounts of the adsorbates were measured in a calibrated volume prior to contact with the zeolite. To equilibrate the adsorbed molecules, the sealed samples were heated at temperatures ranging from 333 to 523 K. The temperatures were high enough to allow rapid redistribution of molecules within the samples but not high enough to cause chemical reactions.

All PFG NMR experiments were performed on a Varian INOVA 400 spectrometer equipped with an ultra high intensity pulsed field gradient facility. An ultrashielded Doty PFG diffusion probe was used. For binary systems, the two components were distinguished by use of the ^{19}F resonance frequency for CF_4 and the ^1H frequency for the hydrocarbons. To avoid the effects of the background gradient on the measured diffusivity, the 13-interval PFG NMR pulse sequence with bipolar-gradient pair (BPP) suggested by Cotts et al.[29] was used to measure the self-diffusivity. The resonance frequencies of ^1H and ^{19}F nuclei were 400.6 and 377.0 MHz, and the corresponding $\pi/2$ pulse widths were 15 and 20 μs, respectively. To remove the cross term between the background gradient and the pulsed field gradient, the delay time prior to the gradient pulse was equal to that after the gradient pulse.[22,25,29] The delay values varied between 200 and 300 μs, depending on the strength and width of the applied gradient pulse. Preliminary experiments indicated that the residual eddy current was negligible under these conditions. Diffusion times varied from about 2 to 18 ms. The gradient pulse widths ranged from 200 μs to 1 ms, depending on the diffusivity, and the gradient intensities went as high as 250 Gauss/cm. 64−224 scans were accumulated depending on the loading amount and the type of the adsorbed molecules. Prior to the acquisition of NMR signals, the adsorbed sample was equilibrated for at least 20 min at the desired temperature of 298 K. The error in temperature was less than 0.1 K.

3. Experimental Data Analysis

When molecules adsorbed in small particles move to the edges of a particle, they generally have two fates: they are either "reflected" back into the particle interior, or they are "absorbed" at the boundary and escape into the intercrystalline space.[22,24] Figure 2 shows these two limiting cases schematically. The escape rates of molecules from the particles depend on the type of molecule, the temperature, the pore dimension, and the external surface properties of the crystals.[1,22] If the transport resistances at the outer surface of the crystals (heat of desorption and any additional surface barriers) are strong enough, the fraction of molecules escaping into the gas phase is negligible, and the molecules are effectively restricted to the particle interiors. Viewed from inside the particle, the surface acts as a reflecting wall, and this case is called the reflecting boundary condition (Figure 2A).[22,24] The other limiting case is that the weak surface resistance cannot effectively confine the probe molecules in the pores, so that many escape into the surrounding atmosphere. This case is called the absorbing boundary condition (Figure 2B).[22,24]

If all adsorbed molecules are confined to the particles during the millisecond NMR observation time, then the molecular displacement is dependent on only one intracrystalline self-diffusion coefficient.[1,22] When the 13-interval PFG NMR

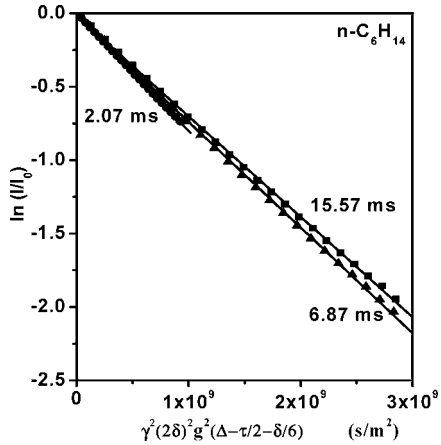

Figure 3. Attenuation curves for the *n*-hexane NMR signal in NaX zeolites loaded with one CF_4 and one *n*-hexane per supercage at different diffusion times. The solid lines represent the fitted results using eq 1.

technique is used, the attenuation of the NMR signal (I) will follow the equation[22,25,29]

$$\ln(I/I_0) = -\gamma^2 D(2\delta)^2 g^2 t \quad (1)$$

where I_0 is the NMR signal intensity without the gradient pulse, γ is the gyromagnetic ratio, δ is the gradient pulse width, g is the gradient pulse intensity, and t is the diffusion time. Here, $t = \Delta - \tau/2 - \delta/6$, where Δ refers to the interval between two gradient pulses with the same direction and τ is the spacing between the first $\pi/2$ RF pulse and the succeeding π RF pulse. According to eq 1, the logarithm of the NMR signal intensity decreases linearly with increasing gradient intensity squared, and the slope of the decay is dependent on the molecular self-diffusivity. For the reflecting boundary condition involving a single diffusivity, only a single-exponential decay line is observed in a plot of $\ln(I/I_0)$ versus the varying gradient pulse intensity squared.

For the absorbing boundary conditions, molecules may wander in two regions during the observation time, including the zeolite pores and the intercrystalline region.[1] The self-diffusivity in nanoporous materials is usually at least several orders smaller than that in the gas phase.[1] The attenuation curve of the NMR signal is therefore governed by two self-diffusion coefficients, and eq 1 cannot describe this case. Thus, another equation, based on a "two-region" approximation model, was used.[1] According to this model, if the 13-interval PFG NMR technique is used, the NMR signal decay will follow the equation[1,25]

$$\ln(I/I_0) = -\gamma^2(2\delta)^2 g^2 [D + p_{\text{inter}} D_{\text{inter}} / (\gamma^2(2\delta)^2 g^2 \tau_{\text{intra}} p_{\text{inter}} D_{\text{inter}} + 1)] t \quad (2)$$

where p_{inter} is the fraction of molecules in the gas phase, D_{inter} is the intercrystalline diffusivity, $p_{\text{inter}}D_{\text{inter}}$ represents the long-range diffusivity, and τ_{intra} is the intracrystalline mean lifetime of molecules. The intracrystalline self-diffusivity D can be obtained by fitting the NMR signal decay curve using eq 2.

For both the reflecting boundary condition and the absorbing boundary condition, a fraction of the molecules always sense the crystalline border during the millisecond diffusion time in micrometer-sized particles. This causes the apparent self-diffusivity (D) detected by PFG NMR to be dependent on the chosen diffusion time.[1,22−24] Only for molecular diffusion times approaching zero are the molecular displacements so short that the adsorbed molecules do not sense the external surface.[22−24] The self-diffusivity corresponding to nearly zero diffusion time is called the unrestricted intracrystalline self-diffusivity and will be denoted as D_0. It is a property related to the adsorbed species, the zeolite, the component composition, and the temperature, but not the experimental diffusion time or the particle size.[22−24] Mitra et al.[23,24] related the measured apparent diffusivities (D) to D_0 for spherical particles. Figure 1 reveals that the NaX crystals have the expected octahedral morphology. To use the spherical model, we set the surface-to-volume (S/V) ratio of the NaX crystals to that of a sphere and calculated the radius R. For the reflecting boundary condition and the absorbing boundary condition, the apparent self-diffusivity of molecules adsorbed in spherical crystals can be described by eqs 3 and 4,[23,24] respectively.

$$D = D_0 - [4/(3R\pi^{1/2})]D_0^{3/2}t^{1/2} - [1/(2R^2)]D_0^2 t \quad (3)$$

$$D = D_0 - [2/(3R\pi^{1/2})]D_0^{3/2}t^{1/2} - (1/R^2)D_0^2 t \quad (4)$$

By fitting the variation of the detected diffusivities (D) with the diffusion times, D_0 can be obtained by extrapolating to zero diffusion time. Using random walk simulations of diffusion in spherical geometries, Mitra et al.[23,24] demonstrated that eqs 3 and 4 apply when the ratio of D/D_0 is larger than 0.5.

4. Multicomponent Diffusion Model

One of our main objectives is to use single-component and mixture self-diffusivities from PFG NMR measurements to test a scheme from the literature developed to predict mixture self-diffusivities from single-component data. In particular, we will test the scheme of Skoulidas, Sholl, and Krishna,[17] which is based on the Maxwell−Stefan formulation of diffusion. Only a brief summary of the method is given here. Readers interested in background, derivations, or more detail are referred to the literature.[17,30] Note that in this section, we drop the subscript 0, which signified above that the self-diffusivity was the "true" intracrystalline value obtained at short measurement times; thus D_i is the true self-diffusivity of species i.

For a single-component system, the Maxwell−Stefan (MS) diffusion coefficient of species i ($Đ_i$) is taken to depend on concentration as follows:

$$Đ_i(\theta) = Đ_i(0)[1 - \theta_i] \quad (5)$$

where $Đ_i(0)$ is the MS diffusivity at zero loading. The fractional loadings are defined as

$$\theta_i = n_i/n_{i,\text{sat}} \quad (6)$$

where n_i and $n_{i,\text{sat}}$ are the loading and the saturation loading of species i, respectively. An inverse friction coefficient $Đ_{ii}$ for friction between particles of the same species is defined as

$$\frac{1}{D_i} = \frac{1}{Đ_i} + \frac{\theta}{Đ_{ii}} \tag{7}$$

Following results from MD simulations for *n*-alkanes and CF_4 in faujasite by Chempath et al.,[30] we take $Đ_{ii}(\theta)$ to be 0.8 $Đ_i(\theta)$. Using this relation in eq 7, we can obtain $Đ_i(\theta)$ from the self-diffusivity $D_i(\theta)$. Using eq 5, $Đ_i(0)$ can be obtained.

From the single-component information, the mixture self-diffusivity can be calculated as follows. First, eq 5 is generalized for mixtures:

$$Đ_i(\theta) = Đ_i(0)[1 - \theta_1 - \theta_2 - ... \theta_n] \tag{8}$$

Using this equation, $Đ_i(\theta)$ in the mixture can be calculated from $Đ_i(0)$ for each component. We again assume that $Đ_{ii} = 0.8Đ_i$. One of the key equations in the method of Skoulidas, Sholl, and Krishna[17] is the logarithmic interpolation to obtain $Đ_{ij}$ (the inverse friction coefficient between species *i* and species *j*) from the values of $Đ_{ii}$ and $Đ_{jj}$:

$$n_{j,\mathrm{sat}}Đ_{ij} = (n_{j,\mathrm{sat}}Đ_{ii})^{n_i/(n_i+n_j)} \times (n_{i,\mathrm{sat}}Đ_{jj})^{n_j/(n_i+n_j)} \tag{9}$$

Finally, the self-diffusivity $D_i(\theta)$ is obtained:

$$\frac{1}{D_i} = \frac{1}{Đ_i} + \sum_{j=1}^{n} \frac{\theta_j}{Đ_{ij}} \tag{10}$$

Thus, the method calculates D_i for mixture conditions using only single-component data as inputs.

5. Results and Discussion

For the binary system loaded with one CF_4 and one *n*-C_6H_{14} per supercage, Figure 3 displays the attenuation of the *n*-hexane NMR signals on a logarithmic scale with increasing gradient intensity squared for three different diffusion times. For each diffusion time, a single straight line is observed, indicating that molecular motion is described by only one diffusion coefficient. In addition, the decay rates of the lines in Figure 3 decrease with increasing diffusion times, and thus the detected *n*-hexane apparent self-diffusivity gradually decreases with increasing diffusion time. Together, these facts show that the *n*-hexane motion in this system is described by the typical reflecting boundary condition. With longer diffusion times, more *n*-hexane molecules will sense the crystal borders and be reflected back by the external surface (see Figure 2A).

Figure 4 shows the attenuation of the CF_4 NMR signals for the binary system loaded with one CF_4 and one CH_4 per supercage at various diffusion times. The signal decays in Figure 4 are not straight lines but curves, which means that there are possibly two CF_4 diffusivities governing molecular motion as discussed above (see Figure 2B).[1] One is a large intercrystalline diffusivity, mainly affecting the fast decay of the NMR signal at low gradient intensities (the long-range diffusivity). The other is a smaller intracrystalline diffusivity, corresponding to the slow decay of the NMR signal at higher gradient intensities. The two-region model (eq 2) was used to fit the decay curves, and the fitted results are shown as solid lines in Figure 4. The excellent agreement between the experimental data and the fit strongly supports the two-region approximation model for this system. Because many CF_4 molecules escape into the intercrystalline space, CF_4 diffusion in this system belongs to the absorbing boundary condition case. Similar results were also observed by Geier et al. for this system.[22] Our results reveal that in all cases investigated here, CF_4 adsorbed in NaX zeolites is described by absorbing boundary conditions. The apparent intracrystalline diffusivity in the pores can be obtained for absorbing boundary condition cases using the two-region model[1,31] (see eq 2). The results in Figures 3 and 4 demonstrate that the boundary conditions for the adsorbed molecules can be obtained from the decay curves of the NMR signals. The intracrystalline self-diffusivities in the other systems were obtained using the two methods above (figures not shown).

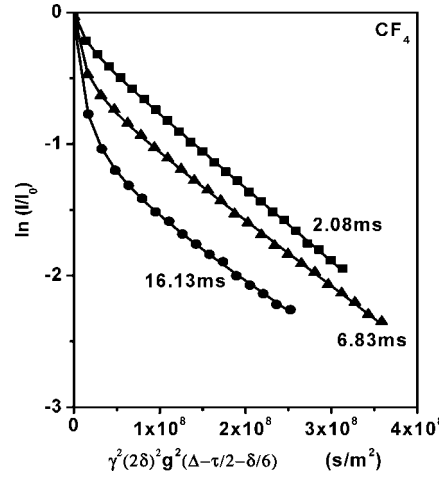

Figure 4. Attenuation curves for the CF_4 NMR signal in NaX zeolites loaded with one CF_4 and one CH_4 per supercage at different diffusion times. The solid lines represent the fitted results using the two-region approximation model.

For the binary system loaded with one CF_4 and one *n*-hexane per supercage, the diffusive motions of CF_4 and *n*-hexane are described by absorbing and reflecting boundary conditions, respectively. Figures 5 and 6 show their apparent intracrystalline diffusivities versus the square root of the diffusion time. With increasing diffusion times, the apparent diffusivities of CF_4 and *n*-hexane both decrease as more and more adsorbed molecules have a chance to encounter the external crystal surface.[22,25−27] To remove this effect, the unrestricted self-diffusivities (D_0) at zero diffusion time were calculated. The short-time diffusion equations (see eqs 3 and 4)[22−24] were used to fit the data in Figures 5 and 6 (solid lines). The reasonable fit of the data means that the variation of apparent diffusivities with diffusion time can be effectively described by the equation suggested by Mitra for both cases, and the unrestricted diffusivities (D_0) estimated in this way should be reliable.[22−24] Extrapolating the solid lines in Figures 5 and 6 to zero diffusion time (see the dashed lines and the solid circles in Figures 5 and 6), we obtained that D_0 of CF_4 and *n*-hexane are 2.2×10^{-9} and 8.4×10^{-10} m^2/s, respectively. The D/D_0 ratios for CF_4 and *n*-hexane in Figures 5 and 6 are greater than 0.7 for all investigated diffusion times, which accords with the requirement that D/D_0 be greater than 0.5 for the short-time diffusion model to effectively describe the apparent diffusivities.[24] The unrestricted diffusivities for the other systems are shown in Tables 1 and 2. In all cases, D/D_0 is greater than 0.5.

Table 1 lists the unrestricted diffusivities for the pure component systems. It can be seen that the diffusivities of the *n*-alkanes decrease with increasing chain length in agreement with previous measurements[32] and MD simulation.[20,33] Figure

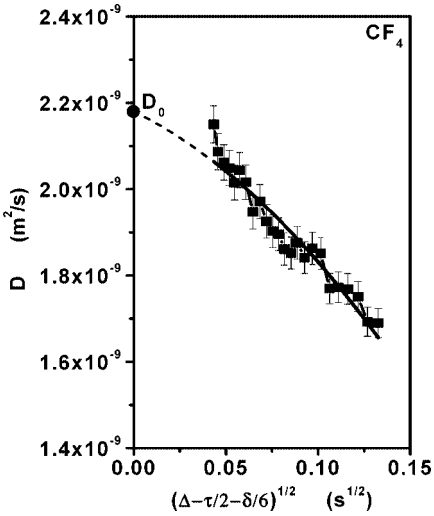

Figure 5. Variation of apparent intracrystalline diffusivities (D) of CF_4 with the square root of the diffusion times for the binary system loaded with one CF_4 and one n-hexane per supercage. The solid line represents the fitted result using eq 4, and the dashed line represents its extrapolation to zero diffusion time. The "●" corresponds to the unrestricted intracrystalline self-diffusivity (D_0) at zero diffusion time.

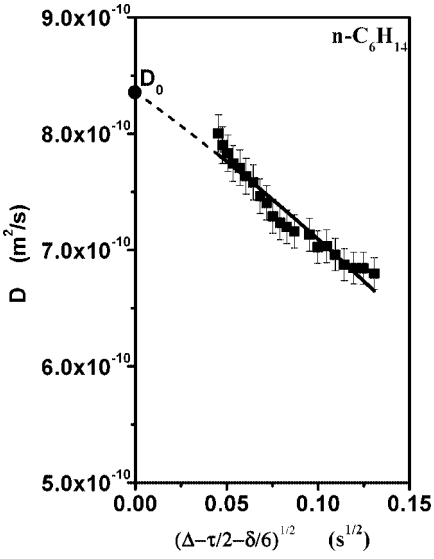

Figure 6. Variation of apparent intracrystalline diffusivities (D) of n-hexane with the square root of the diffusion time for the binary system loaded with one CF_4 and one n-hexane per supercage. The solid line represents the fitted result using eq 3, and the dashed line represents its extrapolation to zero diffusion time. The "●" corresponds to the unrestricted intracrystalline self-diffusivity (D_0) at zero diffusion time.

7 presents the unrestricted self-diffusivities for mixtures containing one CF_4 molecule and one n-alkane (C_1-C_8) molecule per supercage along with the single-component self-diffusivities at a loading of one molecule per supercage. The n-alkane diffusivities in the mixtures are almost identical to the single-component results. The CF_4 diffusivities, on the other hand, decrease significantly when coadsorbed with slower n-alkanes. Thus, the CF_4 diffusivity with coadsorbed methane is essentially the same as for pure CF_4, but when n-octane is coadsorbed, the diffusivity drops by a factor of 6. These trends are consistent with a previous MD simulation[20] for CF_4 and n-alkanes in a siliceous faujasite zeolite. The results also agree with previous observations that for mixtures adsorbed in zeolites, the faster

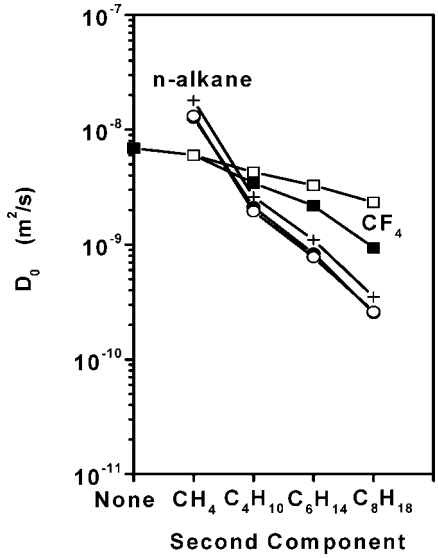

Figure 7. Variation of the unrestricted intracrystalline self-diffusivities (D_0) in binary systems loaded with one CF_4 (squares) and one n-alkane (circles) per supercage. Single-component values for the n-alkanes at a loading of one molecule per supercage are also presented (+). The solid and open symbols represent the self-diffusivities obtained from PFG NMR mixture measurements and the MS estimation scheme, respectively.

species is slowed relative to its pure-component self-diffusivity, while the slower species is unaffected or somewhat speeded up.[4,7] It should be kept in mind that the mixture results in Figure 7 are at constant number of molecules per supercage, but n-octane occupies significantly more space than methane or CF_4. This reduction in free volume can be expected to play a role in reducing the self-diffusivity of CF_4 when coadsorbed with n-octane in addition to the fact that n-octane itself has a lower diffusivity, which will also slow coadsorbed CF_4 molecules through collisions and slower creation of vacancies.[34,35]

Figure 8 presents the unrestricted self-diffusivities for binary systems loaded with one CF_4 and one C_6 hydrocarbon (n-hexane, cyclohexane, or benzene) per supercage along with the single-component diffusivities at a loading of one C_6 hydrocarbon or CF_4 per supercage. Similar to Figure 7, the diffusivity value of the slower species in the binary system is very close to its pure-component diffusivity. (See Figure 8 and Tables 1 and 2.) n-Hexane diffuses slightly faster than cyclohexane, and benzene diffuses more than an order of magnitude more slowly. In Figure 8, the diffusivity of coadsorbed CF_4 follows the same trend: n-hexane > cyclohexane > benzene. n-Hexane, cyclohexane, and benzene have similar molecular volumes.[36,37] The benzene self-diffusivity is much lower than that for n-hexane or cyclohexane due to strong interactions between the aromatic ring of benzene and the sodium cations in the zeolite.[1,38−41] Similar to the trend in Figure 7, the faster component (CF_4) is slowed by the slower and bulkier C_6 molecules.

Another interesting comparison can be made from the experimental data in Table 2. The CF_4 diffusivities in the binary systems containing n-octane and benzene are 9.4×10^{-10} and 8.7×10^{-10} m^2/s, respectively. These very similar CF_4 diffusivities are observed even though the n-octane diffusivity is over 10 times larger than that of benzene in both the pure-component and the binary systems (see Tables 1 and 2). This is presumably due to the larger molecular volume of n-octane as compared to that of benzene.[36,37] n-Octane can block CF_4 motion in the pores, resulting in a similar CF_4 diffusivity as in the case of the much slower but less bulky benzene.

TABLE 1: Single-Component Data in NaX Zeolites at 298 K: Saturation Loadings n_{sat}, Measured Unrestricted Intracrystalline Self-Diffusivities D_0, the Maxwell−Stefan Diffusivities $Đ_i$, and the Maxwell−Stefan Diffusivities at Zero Loading $Đ_i(0)$

loading (molecules/s.c.)[a]	n_{sat}(molecules/s.c.)[a]	θ	D_0 (m^2/s)	$Đ_i$ (m^2/s)	$Đ_i(0)$ (m^2/s)
$1CF_4$	6.8[b]	0.147	6.9×10^{-9}	8.2×10^{-9}	9.6×10^{-9}
$2CF_4$	6.8[b]	0.294	5.1×10^{-9}	7.0×10^{-9}	9.9×10^{-9}
$1CH_4$	14.7[b]	0.068	1.8×10^{-8}	2.0×10^{-8}	2.1×10^{-8}
$1C_4H_{10}$	5.3[b]	0.189	2.6×10^{-9}	3.3×10^{-9}	4.0×10^{-9}
$2C_4H_{10}$	5.3[b]	0.378	1.6×10^{-9}	2.4×10^{-9}	3.8×10^{-9}
$1C_6H_{14}$	3.8[c]	0.263	1.1×10^{-9}	1.4×10^{-9}	1.9×10^{-9}
$1C_8H_{18}$	3.06[d]	0.327	3.5×10^{-10}	4.9×10^{-10}	7.3×10^{-10}
$1C_6H_{12}$	4.5[e]	0.222	8×10^{-10}[e]	1.0×10^{-9}	1.3×10^{-9}
$1C_6H_6$	4.5[f]	0.222	1.3×10^{-11}[g]	1.7×10^{-11}	2.1×10^{-11}

[a] s.c. = supercage. [b] Reference 30. [c] Reference 42. [d] From molecular simulation. [e] Reference 43. [f] Reference 41. [g] Reference 1.

TABLE 2: Comparison of the Unrestricted Intracrystalline Self-Diffusivities from PFG NMR Measurements and from the Maxwell−Stefan Estimation Scheme for Binary Systems in NaX at 298 K

loading	CF_4 (m^2/s)		second component (m^2/s)	
(molecules/s.c.)[a]	MS	PFG NMR	MS	PFG NMR
$1CF_4 + 1CH_4$	6.0×10^{-9}	6.0×10^{-9}	1.3×10^{-8}	1.3×10^{-8}
$1CF_4 + 1C_4H_{10}$	4.3×10^{-9}	3.4×10^{-9}	1.9×10^{-9}	2.1×10^{-9}
$1CF_4 + 1C_6H_{14}$	3.3×10^{-9}	2.2×10^{-9}	7.8×10^{-10}	8.4×10^{-10}
$1CF_4 + 1C_8H_{18}$	2.3×10^{-9}	9.4×10^{-10}	2.6×10^{-10}	2.5×10^{-10}
$1CF_4 + 1C_6H_{12}$	3.4×10^{-9}	1.7×10^{-9}	6.1×10^{-10}	5.7×10^{-10}
$1CF_4 + 1C_6H_6$	1.0×10^{-9}	8.7×10^{-10}	1.0×10^{-11}	1.6×10^{-11}

[a] s.c. = supercage.

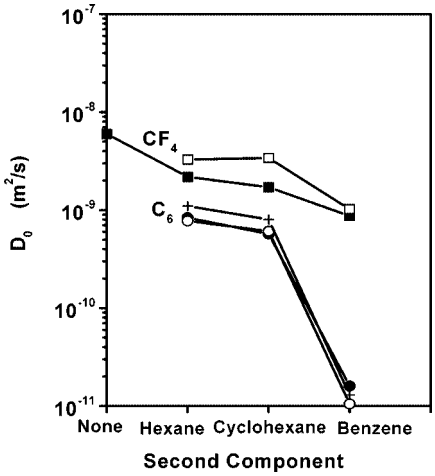

Figure 8. Variation of the unrestricted intracrystalline self-diffusivities (D_0) in binary systems loaded with one CF_4 (squares) and one C_6 hydrocarbon (circles) per supercage. Single-component values for the C_6 hydrocarbons at a loading of one molecule per supercage are also presented (+). The solid and open symbols represent the self-diffusivities obtained from PFG NMR mixture measurements and the MS estimation scheme, respectively.

In addition to the self-diffusivities measured by PFG NMR in mixture samples (solid symbols), Figures 7 and 8 also display the results predicted by the MS estimation scheme using only single-component data as inputs (open symbols). Input data for the pure components in NaX are listed in Table 1. This includes the unrestricted self-diffusivities D_0 measured in this work, saturation loading amounts taken from the literature,[1,30,41−43] and the calculated fractional occupancies θ. With this input, $Đ_i$, $Đ_{ii}$, and $Đ_i(0)$ in the pure components were calculated in order with eqs 7 and 5 as described above (see Table 1). $Đ_i(0)$ at zero loading is a constant for single-components and mixtures, only dependent on the species i, the zeolite, and the temperature. Based on the obtained $Đ_i(0)$ in Table 1, in the multicomponent

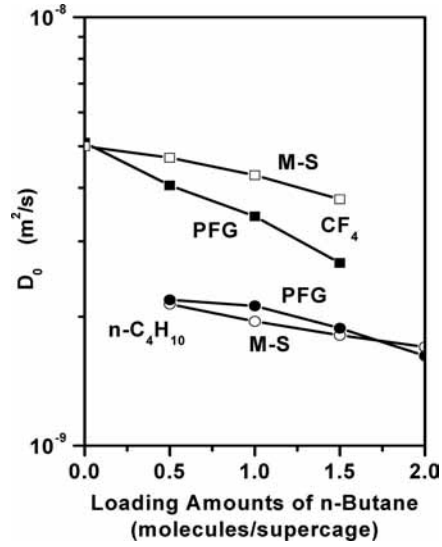

Figure 9. Variation of the unrestricted intracrystalline self-diffusivities (D_0) in binary systems loaded with $n$$CF_4$ (squares) and $(2 - n)$butane (circles) per supercage. The solid and open symbols represent the self-diffusivities obtained from PFG NMR mixture measurements and the MS estimation scheme, respectively.

systems the values of $Đ_i$, $Đ_{ii}$, $Đ_{ij}$, and $D_i(\theta)$ were calculated one by one using eqs 8−10. The binary unrestricted self-diffusivities calculated in this way $D_i(\theta)$ are presented in Figures 7 and 8 and Table 2. It can be seen that the estimated results from the MS scheme are consistent with the measured self-diffusivities within reasonable errors, providing an experimental validation of the MS scheme proposed by Skoulidas, Sholl, and Krishna.[17] This scheme has been tested numerous times using results from MD simulation, but there are few instances of systematic experimental data available for mixtures in zeolites to allow such a test using experimental data. As a self-consistency test, note that the values of $Đ_i(0)$ obtained for pure CF_4 and n-butane at two different loadings in Table 1 are the same within experimental error.

Figure 9 shows results for binary systems loaded with CF_4 and n-butane at a constant total loading of 2 molecules per supercage but varying composition. Again, the results predicted from pure-component data using the MS estimation scheme agree well with the unrestricted self-diffusivities measured directly for the mixtures, providing further validation for the prediction method. The results in Figure 9 show that the diffusivities of both CF_4 and n-butane slowly decrease with an increasing percentage of n-butane. n-Butane is both larger and has a lower pure-component diffusivity (see Table 1 and Figure 9), so as CF_4 molecules are replaced by n-butane molecules, the mixture self-diffusivities of both CF_4 and n-butane decrease.

6. Conclusions

Self-diffusion coefficients of CF_4 and various hydrocarbons in NaX zeolites were measured by PFG NMR for single components and binary mixtures. The variation of the NMR signal with the gradient pulse intensity allowed a clear discrimination between reflecting and absorbing boundary conditions at the crystal edges. For the absorption boundary condition, the well-established two-region model was used to obtain the apparent intracrystalline self-diffusivity. With increasing diffusion time, the apparent diffusivities gradually decrease as molecules approaching the crystal edges are reflected back into the crystal or escape into the gas phase. The true unrestricted intracrystalline self-diffusivities (D_0) were derived by extrapolating to zero diffusion time when no molecules can sense the external surface using the short-time diffusion model.

The intracrystalline self-diffusivity for a given component coadsorbed in a zeolite with a second component is influenced by the diffusivity of the second component and its size. For example, the diffusivity of CF_4 is reduced when the coadsorbed molecules are larger and/or slowly diffusing. The systematic set of mixture data obtained in this study was used to test a scheme for estimating binary diffusion coefficients from single-component data based on the Maxwell−Stefan formulation of diffusion. For mixtures of CF_4 and various hydrocarbons, the self-diffusivities estimated from this method were consistent with those directly measured by PFG NMR experiments for the mixtures. This estimation method has been tested previously by using data from MD simulations. This work provides a critical test using experimentally measured mixture data.

Acknowledgment. This work was supported by the National Science Foundation (CTS-0302428) and the Department of Energy through the Northwestern University Institute for Catalysis in Energy Processes. We thank Dr. G. Joseph Ray, Dr. Yoo Joong Kim, and Dr. Shaji Chempath for helpful discussions and the late Dr. George T. Kokotailo for providing the large-crystal zeolite sample.

References and Notes

(1) Kärger, J.; Ruthven, D. M. *Diffusion in Zeolites and Other Microporous Solids*; Wiley: New York, 1992.
(2) Chen, N. Y.; Degnan, T. F., Jr.; Smith, C. M. *Molecular Transport and Reaction in Zeolites*; VCH: New York, 1994.
(3) Chen, Y. D.; Yang, R. T. *Stud. Surf. Sci. Catal.* **1997**, *104*, 487.
(4) Hong, U.; Kärger, J.; Pfeifer, H. *J. Am. Chem. Soc.* **1991**, *113*, 4812.
(5) Nivarthi, S. S.; McCormick, A. V. *J. Phys. Chem.* **1995**, *99*, 4661.
(6) Nivarthi, S. S.; Davis, H. T.; McCormick, A. V. *Chem. Eng. Sci.* **1995**, *50*, 3217.
(7) Snurr, R. Q.; Kärger, J. *J. Phys. Chem. B* **1997**, *101*, 6469.
(8) Jost, S.; Bär, N. K.; Fritzsche, S.; Haberlandt, R.; Kärger, J. *J. Phys. Chem. B* **1998**, *102*, 6375.
(9) Schuring, D.; Koriabkina, A. O.; de Jong, A. M.; Smit, B.; van Santen, R. A. *J. Phys. Chem. B* **2001**, *105*, 7690.
(10) Gergidis, L. N.; Theodorou, D. N.; Jobic, H. *J. Phys. Chem. B* **2000**, *104*, 5541.
(11) Jiang, M.; Eic, M. *Adsorption* **2003**, *9*, 225.
(12) Brandani, S.; Jama, M.; Ruthven, D. M. *Ind. Eng. Chem. Res.* **2000**, *39*, 821.
(13) Carlson, N. W.; Dranoff, J. S. Competitive adsorption of methane and ethane on 4A zeolite. In *Fundamentals of Adsorption*; Liapis, A. I., Ed.; Engineering Foundation:New York, 1986; p 129.
(14) Yasuda, Y.; Matsumoto, K. *J. Phys. Chem.* **1989**, *93*, 3195.
(15) Yang, R. T.; Chen, Y. D.; Yeh, Y. T. *Chem. Eng. Sci.* **1991**, *46*, 3089.
(16) Yang, R. T.; Sikavitsas, V. I. *Chem. Eng. Sci.* **1995**, *50*, 3319.
(17) Skoulidas, A. I.; Sholl, D. S.; Krishna, R. *Langmuir* **2003**, *19*, 7977.
(18) Krishna, R.; Baur, R. *Sep. Purif. Technol.* **2003**, *33*, 213.
(19) Krishna, R.; Paschek, D. *Phys. Chem. Chem. Phys.* **2002**, *4*, 1891.
(20) Sanborn, M. J.; Snurr, R. Q. *Sep. Purif. Technol.* **2000**, *20*, 1.
(21) Dubbeldam, D.; Snurr, R. Q. *Mol. Simul.* **2007**, *33*, 305.
(22) Geier, O.; Snurr, R. Q.; Stallmach, F.; Kärger, J. *J. Chem. Phys.* **2004**, *120*, 367.
(23) Mitra, P. P.; Sen, P. N.; Schwartz, L. M.; Ledoussal, P. *Phys. Rev. Lett.* **1992**, *68*, 3555.
(24) Mitra, P. P.; Sen, P. N.; Schwartz, L. M. *Phys. Rev. B* **1993**, *47*, 8565.
(25) Courivaud, F.; Hansen, E. W.; Kolboe, S.; Karlsson, A.; Stocker, M. *Microporous Mesoporous Mater.* **2000**, *37*, 223.
(26) Gjerdaker, L.; Sorland, G. H.; Aksnes, D. W. *Microporous Mesoporous Mater.* **1999**, *32*, 305.
(27) Kärger, J.; Stallmach, F.; Vasenkov, S. *Magn. Reson. Imaging* **2003**, *21*, 185.
(28) Sorland, G. H. *J. Magn. Reson.* **1997**, *126*, 146.
(29) Cotts, R. M.; Hoch, M. J. R.; Sun, T.; Markert, J. T. *J. Magn. Reson.* **1989**, *83*, 252.
(30) Chempath, S.; Krishna, R.; Snurr, R. Q. *J. Phys. Chem. B* **2004**, *108*, 13481.
(31) Kärger, J.; Pfeifer, H. *Zeolites* **1987**, *7*, 90.
(32) Kärger, J.; Pfeifer, H.; Rauscher, M.; Walter, A. *J. Chem. Soc., Faraday Trans. 1* **1980**, *76*, 717.
(33) Clark, L. A.; Ye, G. T.; Gupta, A.; Hall, L. L.; Snurr, R. Q. *J. Chem. Phys.* **1999**, *111*, 1209.
(34) Krishna, R.; Paschek, D.; Baur, R. *Microporous Mesoporous Mater.* **2004**, *76*, 233.
(35) Krishna, R.; van Baten, J. M. *Microporous Mesoporous Mater.* **2008**, *109*, 91.
(36) Webster, C. E.; Drago, R. S.; Zerner, M. C. *J. Am. Chem. Soc.* **1998**, *120*, 5509.
(37) Xiao, J. R.; Wei, J. *Chem. Eng. Sci.* **1992**, *47*, 1123.
(38) Wu, J. F.; Chen, T. L.; Ma, L. J.; Lin, M. W.; Liu, S. B. *Zeolites* **1992**, *12*, 86.
(39) Ruthven, D. M.; Kaul, B. K. *Ind. Eng. Chem. Res.* **1993**, *32*, 2053.
(40) Ruthven, D. M.; Kaul, B. K. *Ind. Eng. Chem. Res.* **1993**, *32*, 2047.
(41) Jeong, B. H.; Hasegawa, Y.; Sotowa, K. I.; Kusakabe, K.; Morooka, S. *J. Membr. Sci.* **2003**, *213*, 115.
(42) Herden, H.; Einicke, W. D.; Jusek, M.; Messow, U.; Schollner, R. *J. Colloid Interface Sci.* **1984**, *97*, 559.
(43) Kärger, J.; Lorenz, P.; Pfeifer, H.; Bülow, M. *Z. Phys. Chem. (Leipzig)* **1976**, *257*, 209.

JP810058Z